

Latent Augmentation For Better Graph Self-Supervised Learning

Jiashun Cheng^{1,2}, Man Li^{1,2}, Jia Li^{1,2}, Fugee Tsung^{1,2}

¹The Hong Kong University of Science and Technology (Guangzhou)

²The Hong Kong University of Science and Technology
 {jchengak, mlicn}@connect.ust.hk,
 {jialeee, season}@ust.hk

Abstract

Graph self-supervised learning has been vastly employed to learn representations from unlabeled graphs. Existing methods can be roughly divided into predictive learning and contrastive learning, where the latter one attracts more research attention with better empirical performance. We argue that, however, predictive models weaponed with latent augmentations and powerful decoder could achieve comparable or even better representation power than contrastive models. In this work, we introduce data augmentations into latent space for superior generalization and better efficiency. A novel graph decoder named Wiener Graph Deconvolutional Network is correspondingly designed to perform information reconstruction from augmented latent representations. Theoretical analysis proves the superior reconstruction ability of graph wiener filter. Extensive experimental results on various datasets demonstrate the effectiveness of our approach.

1 Introduction

Self-Supervised Learning (SSL) has been extended to graph data recently due to its great success in computer visions, which extracts informative knowledge through well-designed pretext tasks from unlabeled data [39]. With regard to the objectives of pretext tasks, graph SSL can be divided into two major categories: predictive SSL and contrastive SSL [20]. Predictive models train the graph autoencoders with a prediction task supervised by informative properties generated from graph freely, while contrastive models are trained on the mutual information between several different views contrasted from the original graph. As the dominant technique, contrastive SSL has achieved state-of-the-art performance empirically [25, 52] for graph representation learning. However, its high dependence on data augmentation schemes causes critical scaling-up and efficiency issues [42].

In terms of predictive SSL, graph reconstruction is a natural self-supervision. Most methods, e.g., GAE [13], employ autoencoder structure with augmentations on the input graph, like node masking [49] and feature masking[9], to enrich the training data. However, a tiny augmentation on the original

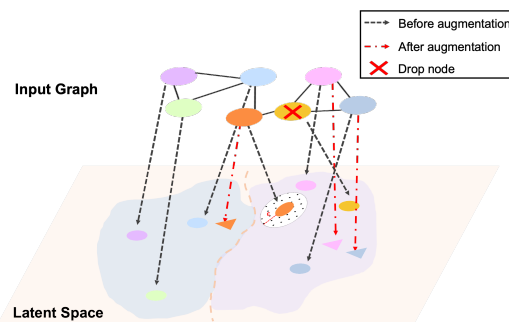


Figure 1: Augmentations on original graph may uncontrollably change the semantics causing wrong classification, whereas augmentations on latent space are continuous and controllable.

graph may unexpectedly cause huge variation on latent space, or even change the semantics. For example, dropping a hub node will change the class manifolds of its neighbors (see Figure 1). In this regard, many commonly used augmentations are semantically uncontrollable and may take the risk of low generalizations. To avoid such semantic ambiguity, one may seek for domain-specific knowledge as guidance, but this will lead to inefficiency. Therefore, a natural question comes up, that is, *can we improve predictive SSL by naïve augmentations for efficient and powerful representation learning?*

Inspired by representation learning [3], we inject simple augmentations (e.g., Gaussian noise) on latent graph representations, which is more likely to capture diverse semantic transformations. It requires no domain knowledge and avoids heuristic data augmentations, and can therefore improve generalization and efficiency. However, the learning paradigm of predictive SSL, especially graph autoencoder, will be severely affected by the additive augmentations and most decoders are vulnerable w.r.t. these additive augmentations, including existing GALA [24] and Graph Deconvolutional Network (GDN) [17]. Therefore, an adaptive decoder for augmented latent space is required. Motivated by recent advancement of wiener in deep image restoration [4], we introduce the classical deconvolutional technique, wiener kernel, into GDN, which is the theoretical optimum for restoring noisy signals with respect to Mean Squared Error (MSE). Specifically, we first derive the graph wiener filter and prove its superiority in theory. We observe that, however, directly using the explicit wiener filter induces low scalability due to indispensable eigen-decomposition and may be not applicable to large-scale datasets. Therefore, we adopt average graph spectral power and Remez polynomial [23] for fast approximation. We evaluate the effectiveness and efficiency of the proposed wiener GDN on node and graph classification tasks with extensive datasets and achieve outperforming performance.

The main contributions of this work are as follows:

- We inject simple augmentations to latent representations efficiently using Gaussian noise, which can enrich the diversity of training data while preserving semantics.
- We develop Wiener Graph Deconvolutional Network (WGDN), in order to better reconstruct graph attributes from augmented latent space.

2 Related work

Graph self-supervised learning According to recent surveys [20, 42], works in graph SSL can be classified into two categories: contrastive learning and predictive learning. Contrastive SSL attracts more attention currently due to the state-of-the-art performance on representation learning empirical evaluations. DGI [36], the pioneer work, incorporates GNN with contrastive learning using local-global mutual information maximization. Within this research line, improvements mainly focus on the augmentation schemes. For example, MVGRL [8] applies graph diffusion to generate structural views. GRACE [51] proposes to generate two augmented views by corruption. GCA [52] further improves it by considering structure and attribute information. Despite their advancement, most of their augmentations rely on domain-specific knowledge and limit their efficiency. As for predictive learning, predicting node attribute and neighborhood context is a traditional pretext task, and its representative manner [49] follows the perturb-then-learn strategy to predict the corrupted information, such as attribute masking [9] and feature corruption [38]. Our work belongs to predictive learning and we, for the first time, propose simple augmentations on latent representations.

Graph deconvolutional network Regarding graph deconvolution, early research [46] formulates the deconvolution as a pre-processing step. GALA [24] and SpecAE [18] both perform Laplacian sharpening to recover information. Recent work [50] employ GCN [14] to reconstruct node attributes from the latent representations. All these works, however, neglect the influence of noise. Another GDN framework [17] is designed via a combination of inverse filters in spectral domain and denoising layers in wavelet domain, which is sub-optimal regarding signal reconstruction. Wiener filtering, as an alternative, executes an optimal trade-off between signal recovering and denoising. It has been introduced to deconvolutional networks [4, 31] for image deblurring. However, its effectiveness on graph structure has not been well investigated yet.

Latent space data augmentation Data augmentations in latent space can enrich semantic transformations which are difficult to be defined in the input space [34]. It has been extensively studied in representation learning, and common manipulations, such as interpolation, extrapolation, random

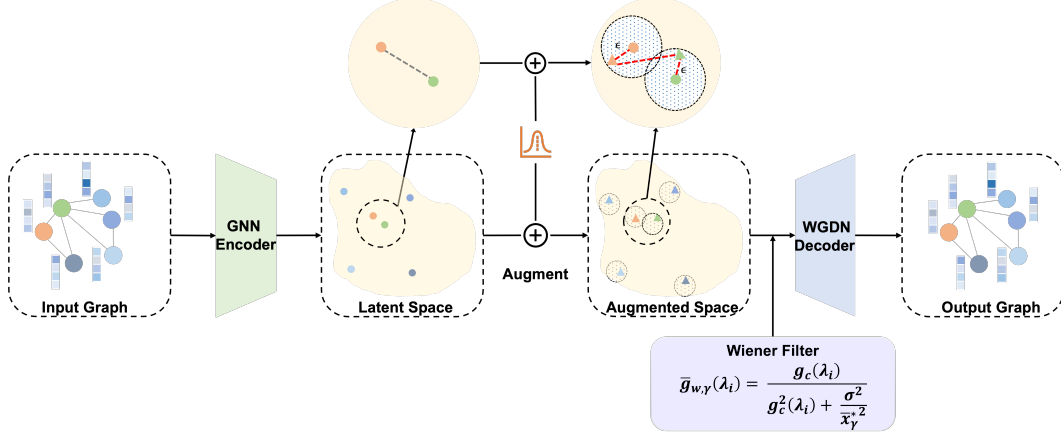


Figure 2: The autoencoder framework for graph SSL with proposed WGDN model. Gaussian noise is introduced adaptively as latent augmentations to enrich the diversity of training data. The proposed WGDN facilitates representation learning with graph wiener filter by recovering information from the augmented latent space.

translation and adding Gaussian noise [3, 2], have shown their effectiveness in CV[19, 37, 32] and NLP [16]. Recently, latent augmentation is introduced in adversarial training [11] for GNNs. Our work will further exploit its potentials in graph SSL.

3 Preliminaries

Under a generic unsupervised graph representation learning setup, we are given an attributed graph $\mathcal{G} = (\mathcal{V}, \mathbf{A}, \mathbf{X})$ consisting of: (1) $\mathcal{V} = \{v_1, v_2, \dots, v_N\}$ is the set of nodes; (2) $\mathbf{A} \in \mathbb{R}^{N \times N}$ is the adjacency matrix where $\mathbf{A}_{ij} \in \{0, 1\}$ represents whether an undirected edge exists between v_i and v_j ; and (3) $\mathbf{X} \in \mathbb{R}^{N \times D}$ denotes the attribute matrix. Our objective is to learn an autoencoder with encoder $\mathcal{E} : (\mathbb{R}^{N \times N}, \mathbb{R}^{N \times D}) \mapsto \mathbb{R}^{N \times D'}$ and decoder $\mathcal{D} : \mathbb{R}^{N \times D'} \mapsto (\mathbb{R}^{N \times N}, \mathbb{R}^{N \times D})$ to produce semantic node embedding. $\mathbf{H} = \mathcal{E}(\mathbf{A}, \mathbf{X}) \in \mathbb{R}^{N \times D'}$ represents the learned embedding in low dimensional space, which can be used for various downstream tasks.

Graph convolution Convolutional operation in graph can be interpreted as a special form of Laplacian smoothing on nodes. From the spectral perspective, graph convolution on a signal $\mathbf{x} \in \mathbb{R}^N$ with a filter g_c is defined as

$$\begin{aligned} \mathbf{h} &= g_c * \mathbf{x} = \mathbf{U} \text{diag}(g_c(\lambda_1), \dots, g_c(\lambda_N)) \mathbf{U}^T \mathbf{x} \\ &= \mathbf{U} g_c(\mathbf{\Lambda}) \mathbf{U}^T \mathbf{x} = g_c(\mathbf{L}) \mathbf{x}, \end{aligned} \quad (1)$$

where $\{\lambda_i\}_{i=1}^N$ and \mathbf{U} represent the eigenvalues and eigenvectors of normalized Laplacian matrix $\mathbf{L} = \mathbf{I} - \mathbf{D}^{-\frac{1}{2}} \mathbf{A} \mathbf{D}^{-\frac{1}{2}} = \mathbf{U} \mathbf{\Lambda} \mathbf{U}^T$ respectively. \mathbf{D} denotes the Degree matrix. $*$ denotes convolutional operator. We consider (1) GCN [14], it is a low-pass filter in spectral domain with $g_c(\lambda_i) = 1 - \lambda_i$ shown by [41]; (2) GDC [15], it uses heat diffusion kernel $g_c(\lambda_i) = e^{-t\lambda_i}$; (3) APPNP [5], it leverages personalized pagerank kernel $g_c(\lambda_i) = \frac{\alpha}{1 - (1 - \alpha)(1 - \lambda_i)}$.

Graph deconvolution As an inverse to convolution, graph deconvolution aims to recover the input attributes given the smoothed node representation. From the spectral perspective, graph deconvolution on a smoothed representation $\mathbf{h} \in \mathbb{R}^N$ with filter g_d is defined as

$$\begin{aligned} \hat{\mathbf{x}} &= g_d * \mathbf{h} = \mathbf{U} \text{diag}(g_d(\lambda_1), \dots, g_d(\lambda_N)) \mathbf{U}^T \mathbf{h} \\ &= \mathbf{U} g_d(\mathbf{\Lambda}) \mathbf{U}^T \mathbf{h} = g_d(\mathbf{L}) \mathbf{h}. \end{aligned} \quad (2)$$

A trivial selection of g_d is the inverse function of g_c , e.g., $g_d(\lambda_i) = \frac{1}{1 - \lambda_i}$ for GCN [17], $g_d(\lambda_i) = e^{t\lambda_i}$ for GDC, or $g_d(\lambda_i) = \frac{1 - (1 - \alpha)(1 - \lambda_i)}{\alpha}$ for APPNP.

4 The proposed framework

In this section, we first extend classical wiener filter to graph domain and demonstrate its superiority in handling augmented representations. Then, we propose Wiener Graph Deconvolutional Network (WGDN), an efficient training scheme weaponed with latent augmentations and graph wiener filter.

4.1 Wiener filter on graph

In this work, we follow the settings in previous papers [11, 2] and introduce additive latent augmentations in model training due to its flexible statistical characteristics. Combining with the graph convolution in Eq. 1, augmented representation $\hat{\mathbf{h}}$ in graph is similarly defined as

$$\hat{\mathbf{h}} = \mathbf{U}g_c(\mathbf{\Lambda})\mathbf{U}^T\mathbf{x} + \epsilon, \quad (3)$$

where $\mathbf{x} \in \mathbb{R}^N$ denotes input attribute and $\epsilon \in \mathbb{R}^N$ is assumed to be any *i.i.d.* random augmentation with $\mathbb{E}[\epsilon_i] = 0$ and $\text{VAR}[\epsilon_i] = \sigma^2$. In contrast to the isolated data augmentations in graph topology and features, ϵ indirectly represents joint augmentations to both [11]. Naturally, attribute recovered by graph deconvolution is formulated by

$$\hat{\mathbf{x}} = \mathbf{U}g_d(\mathbf{\Lambda})g_c(\mathbf{\Lambda})\mathbf{U}^T\mathbf{x} + \mathbf{U}g_d(\mathbf{\Lambda})\mathbf{U}^T\epsilon. \quad (4)$$

Proposition 4.1. *Let $\hat{\mathbf{x}}_{inv}$ be recovered attribute by inverse filter $g_d(\lambda_i) = g_c^{-1}(\lambda_i)$. If $g_c : [0, 2] \mapsto [-1, 1]$, then the reconstruction MSE is dominated by amplified augmentation $\text{MSE}(\hat{\mathbf{x}}_{inv}) = \mathbb{E}\|\mathbf{x} - \hat{\mathbf{x}}_{inv}\|_2^2 = \sum_{i=1}^N \frac{\sigma^2}{g_c^2(\lambda_i)}$.*

The proof is trivial and illustrated in Appendix A for details. Based on Proposition 4.1, the reconstruction-based learning scheme towards attributes becomes ineffective if inverse filter is implemented on augmented latent space. Our goal is to facilitate the graph reconstruction with augmented representations, which resembles the classical restoration problems in some sense. In signal deconvolution, classical wiener filter [40] is able to produce a statistically optimal estimation of the real signals from the noisy ones with respect to MSE. With this regard, we are encouraged to extend wiener filter to graph domain [27]. Assuming the augmentation to be independent from input attributes, graph wiener filter can be similarly defined by extending MSE to graph spectral domain

$$\begin{aligned} \text{MSE}(\hat{\mathbf{x}}) &= \mathbb{E}\|\hat{\mathbf{x}} - \mathbf{x}\|_2^2 = \mathbb{E}\|\mathbf{U}^T\hat{\mathbf{x}} - \mathbf{U}^T\mathbf{x}\|_2^2 \\ &= \sum_{i=1}^N (g_d(\lambda_i)g_c(\lambda_i) - 1)^2 \mathbb{E}[x_i^{*2}] + g_d^2(\lambda_i) \mathbb{E}[\epsilon_i^{*2}] \\ &= \sum_{i=1}^N S(\lambda_i, x_i^*, \sigma, g_c, g_d), \end{aligned} \quad (5)$$

where $\mathbf{x}^* = \mathbf{U}^T\mathbf{x} = \{x_1^*, x_2^*, \dots, x_N^*\}$ and $\epsilon^* = \mathbf{U}^T\epsilon = \{\epsilon_1^*, \epsilon_2^*, \dots, \epsilon_N^*\}$ represent graph spectral projection of the input and augmentation. We denote $\mathbb{E}[x_i^{*2}]$ and $S(\lambda_i, x_i^*, \sigma, g_c, g_d)$ as the spectral power and spectral reconstruction error of spectrum λ_i . Considering the convexity of Eq. 5, MSE is minimized by setting the derivative with respect to $g_d(\lambda_i)$ to zero and thus we obtain the graph wiener filter $g_w(\lambda_i)$ as

$$g_w(\lambda_i) = \frac{g_c(\lambda_i)}{g_c^2(\lambda_i) + \sigma^2/\mathbb{E}[x_i^{*2}]}, \quad (6)$$

where $\sigma^2 = \text{VAR}[\epsilon_i^*] = \mathbb{E}[\epsilon_i^{*2}]$ and $\sigma^2/\mathbb{E}[x_i^{*2}]$ is denoted as the Reciprocal of Signal-to-Noise Ratio (RSNR) of particular spectrum λ_i , which represents the relative magnitude of augmentation.

Proposition 4.2. *Let $\hat{\mathbf{x}}_w$ be recovered attribute by $g_w(\lambda_i)$, where $g_w(\lambda_i)$ is a graph wiener filter, then the reconstruction MSE and variance of $\hat{\mathbf{x}}_w$ are less than $\hat{\mathbf{x}}_{inv}$.*

Please refer to Appendix B for details. Proposition 4.2 shows graph wiener filter has better reconstruction property than inverse filter, which promotes the resilience to latent augmentations and permits stable model training. We observe that, in Eq. 2 and 6, eigen-decomposition is indispensable in computations of spectral power and deconvolutional filter. However, in terms of scalability, an important issue for large-scale graphs is to avoid eigen-decomposition. Note that $\sum_{i=1}^N \mathbb{E}[x_i^{*2}] = \sum_{i=1}^N \mathbb{E}[x_i^2]$

due to orthogonal transformation, we propose the modified graph wiener filter $\bar{g}_{w,\gamma}$ with average spectral power $\bar{x}_\gamma^{*2} = \gamma \times \frac{1}{N} \sum_{i=1}^N \mathbb{E}[x_i^{*2}]$ as

$$\bar{g}_{w,\gamma}(\lambda_i) = \frac{g_c(\lambda_i)}{g_c^2(\lambda_i) + \sigma^2/\bar{x}_\gamma^{*2}}, \quad (7)$$

where γ is a hyperparameter to adjust RSNR. As a natural extension of Proposition 4.2, $\bar{g}_{w,\gamma}$ owns the following proposition.

Proposition 4.3. *Let $\hat{\mathbf{x}}_{w,\gamma}$ be the recovered attribute by modified graph wiener filter $\bar{g}_{w,\gamma}(\lambda_i)$, then the variance of $\hat{\mathbf{x}}_{w,\gamma}$ is less than $\hat{\mathbf{x}}_{inv}$. In spectral domain, given two different γ_1, γ_2 such that $\mathbb{E}[x_i^{*2}] \leq \bar{x}_{\gamma_1}^{*2} \leq \bar{x}_{\gamma_2}^{*2}$, the spectral reconstruction error $S(\lambda_i, x_i^*, \sigma, g_c, \bar{g}_{w,\gamma_1}) \leq S(\lambda_i, x_i^*, \sigma, g_c, \bar{g}_{w,\gamma_2}) \leq S(\lambda_i, x_i^*, \sigma, g_c, g_c^{-1})$.*

Please refer to Appendix C for details. Proposition 4.3 demonstrates that $\bar{g}_{w,\gamma}$ attends to spectral reconstructions over different ranges of spectra, depending on the selection of γ . The graph wiener kernel $\mathbf{D}_\gamma = \mathbf{U}\bar{g}_{w,\gamma}(\mathbf{\Lambda})\mathbf{U}^T$ is then reformatted in matrix form as

$$\mathbf{D}_\gamma = \mathbf{U}(g_c^2(\mathbf{\Lambda}) + \frac{\sigma^2}{\bar{x}_\gamma^{*2}}\mathbf{I})^{-1}g_c(\mathbf{\Lambda})\mathbf{U}^T. \quad (8)$$

Note that g_c can be arbitrary function and support of λ_i is restricted to $[0, 2]$, we adopt Remez polynomial [23] to approximate $\bar{g}_{w,\gamma}(\lambda_i)$ to neglect eigen-decomposition and matrix inverse in Eq. 8.

Definition 4.1 (Remez Polynomial Approximation). *Given an arbitrary continuous function $\zeta(t)$ on $t \in [a, b]$, the Remez polynomial approximation for $\zeta(t)$ is defined as*

$$p_K(t) := \sum_{k=0}^K c_k t^k, \quad (9)$$

where coefficients c_0, \dots, c_K and leveled error e are obtained by resolving linear system

$$\zeta(t_j) = p_K(t_j) + (-1)^j e, \quad (10)$$

where $\{t_j\}_{j=0}^{K+1}$ are interpolation points within $[a, b]$.

Lemma 4.1. *If interpolation points $\{t_j\}_{j=0}^{K+1}$ are Chebyshev nodes, the interpolation error $|\zeta(t) - p_K(t)|$ of Remez polynomial $p_K(t)$ is minimized.*

The proof is trivial and illustrated in detail as Corollary 8.11 in [1]. Following Definition 4.1, the K^{th} order Remez approximation of \mathbf{D}_γ is formulated as

$$\mathbf{D}_\gamma = \mathbf{U}p_K(\mathbf{\Lambda})\mathbf{U}^T = \sum_{k=0}^K c_{k,\gamma}\mathbf{L}^k, \quad (11)$$

where \mathbf{D}_γ is approximated adaptively in each epoch.

4.2 Wiener graph deconvolutional network

Graph encoder To incorporate both graph attributes \mathbf{X} and structure \mathbf{A} in a unified framework, we employ M layers of graph convolution neural network as our graph encoder. For $m = 0, \dots, M - 1$,

$$\mathbf{H}^{(m+1)} = \phi(g_c(\mathbf{L})\mathbf{H}^{(m)}\mathbf{W}^{(m)}), \quad (12)$$

where $\mathbf{H}^{(0)} = \mathbf{X}$, ϕ is the activation function such as PReLU and $g_c(\lambda_i) = 1 - \lambda_i$ as in GCN [14], $g_c(\lambda_i) = e^{-t\lambda_i}$ as in GDC [15] or $g_c(\lambda_i) = \frac{\alpha}{1-(1-\alpha)(1-\lambda_i)}$ as in APPNP [5].

Representation augmentation For simplicity, Gaussian noise is employed as latent augmentations to the node embedding generated by the last layer encoder

$$\hat{\mathbf{H}}^{(M)} = \mathbf{H}^{(M)} + \beta\mathbf{E}, \quad (13)$$

where $\mathbf{E} = \{\epsilon_1, \dots, \epsilon_N\}$, $\epsilon_i \sim N(\mathbf{0}, \sigma_P^2\mathbf{I})$, $\sigma_P^2 = \text{VAR}[\mathbf{H}^{(M)}]$ and β is a hyperparameter to adjust the size of augmentations.

Wiener graph decoder The decoder aims to recover original attributes given the augmented representation $\hat{\mathbf{H}}$. Our previous analysis demonstrates the superiority of wiener kernel to permit reconstruction-based representation learning from augmented latent space. Considering the properties of spectral reconstruction error from Proposition 4.3, we symmetrically adopt M layers of graph deconvolution as the decoder, where each layer consists of q channels of wiener kernels. For $m = 1, \dots, M$ and $i = 1, \dots, q$,

$$\begin{aligned}\mathbf{Z}_i^{(m-1)} &= \phi(\mathbf{D}_{\gamma_i}^{(m)} \hat{\mathbf{H}}^{(m)} \mathbf{W}_i^{(m)}), \\ \hat{\mathbf{H}}^{(m-1)} &= \text{AGG}([\mathbf{Z}_1^{(m-1)}, \dots, \mathbf{Z}_q^{(m-1)}]),\end{aligned}\tag{14}$$

where $\hat{\mathbf{X}} = \hat{\mathbf{H}}^{(0)}$ and $\text{AGG}(\cdot)$ is aggregation function such as summation.

Optimization and Inference Our model is optimized following the convention of reconstruction-based SSL mechanism, which is simply summarized as

$$\mathcal{L} = \|\mathbf{X} - \hat{\mathbf{X}}\|_F.\tag{15}$$

For downstream applications, we treat the fully trained $\mathbf{H}^{(M)}$ as the final node embedding. For graph-level tasks, we adopt a non-parametric graph pooling (readout) function \mathcal{R} , e.g. MaxPooling, to generate graph representation $\mathbf{h}_g = \mathcal{R}(\mathbf{H}^{(M)})$.

Complexity analysis The most intensive computational cost of our proposed method is kernel approximation in Eq. 11. Note that kernel approximation is a simple K^{th} order polynomial of graph convolution. By sparse-dense matrix multiplication, graph convolution can be efficiently implemented, which take $O(K|E|D^2)$ [14] for a graph with $|E|$ edges.

Comparison with variational autoencoder In contrast to VGAE [13] which models the distribution of low-dimensional representations as Gaussians, our proposed method has no requirement of data distribution.

Comparison with adversarial training In general, adversarial training scheme comes with a min-max optimization considering regularized perturbations [32, 11]. Differently, our method just involves min optimization and our augmentation aims to enrich the diversity of training samples in latent space.

5 Experiments

In this section, we investigate the benefit of our proposed approach by addressing the following questions:

- **Q1.** Does our proposed WGDN outperform baseline methods?
- **Q2.** Do all key components of WGDN contribute to the representation learning?
- **Q3.** Is WGDN more scalable than baseline methods?
- **Q4.** How do the hyperparameters impact our proposed model?

5.1 Experimental setup

Datasets We conduct experiments on both node-level and graph-level representation learning tasks with benchmark datasets across different scales and domains, including Cora, CiteSeer, PubMed [28], Amazon Computers, Photo [29], Coauthor CS, Physics [29], and IMDB-B, IMDB-M, PROTEINS, COLLAB, MUTAG, DD, NCI1 in TUDataset [21]. To avoid superficial statistical evaluation and overfitting to fixed data split, we leverage random split mechanism [5]. Detailed statistics are in Table 4 of Appendix E.1.

Table 1: Node classification accuracy of all compared methods. The best and runner up models in unsupervised learning are highlighted in boldface and underlined. * denotes Out-of-Memory on a Tesla V100 32G GPU.

Model	Cora	CiteSeer	PubMed	Computers	Photo	CS	Physics
Raw Feat.	47.5 ± 1.9	48.1 ± 2.0	65.8 ± 2.6	64.0 ± 2.5	76.1 ± 1.6	87.3 ± 0.7	88.8 ± 0.9
Node2Vec	68.3 ± 1.6	45.2 ± 1.5	64.6 ± 2.7	74.0 ± 1.6	83.8 ± 1.3	77.0 ± 0.9	79.9 ± 1.5
DeepWalk	69.7 ± 1.8	42.9 ± 1.8	64.6 ± 2.9	77.2 ± 1.3	85.4 ± 1.2	75.3 ± 1.1	80.7 ± 2.0
DeepWalk + Feat.	72.4 ± 1.6	49.5 ± 1.9	66.1 ± 2.8	78.9 ± 1.3	88.0 ± 1.2	88.6 ± 0.6	90.0 ± 0.8
GAE	74.2 ± 1.3	49.3 ± 1.9	77.0 ± 2.2	79.2 ± 1.6	88.9 ± 1.0	84.5 ± 1.3	81.4 ± 2.7
GCN _{AE}	68.1 ± 0.6	58.3 ± 1.7	73.6 ± 3.0	66.9 ± 2.2	82.9 ± 1.5	87.6 ± 0.8	83.4 ± 2.0
GALA	79.8 ± 1.3	65.8 ± 1.2	72.8 ± 3.0	80.2 ± 1.5	88.1 ± 0.9	90.0 ± 0.7	91.3 ± 1.0
GDN	79.7 ± 1.2	66.2 ± 1.5	75.0 ± 2.8	81.3 ± 1.5	89.6 ± 0.9	90.1 ± 0.6	92.1 ± 0.9
DGI	80.0 ± 0.9	70.9 ± 1.2	77.4 ± 2.7	63.6 ± 3.3	77.3 ± 2.3	90.5 ± 0.5	92.6 ± 1.0
MVGRL	<u>81.2 ± 1.0</u>	69.6 ± 1.6	79.0 ± 1.6	76.3 ± 1.7	86.4 ± 1.4	88.1 ± 0.8	90.5 ± 1.4
GRACE	80.1 ± 1.0	70.2 ± 1.3	80.2 ± 1.6	77.9 ± 2.2	89.3 ± 1.2	85.2 ± 0.8	91.8 ± 1.1
GMI	78.8 ± 1.1	<u>70.0 ± 1.3</u>	77.6 ± 2.1	65.2 ± 3.1	85.5 ± 1.6	90.3 ± 0.5	*
GCA	75.4 ± 1.7	67.9 ± 1.4	77.9 ± 3.0	75.0 ± 1.4	76.6 ± 2.7	89.0 ± 0.7	92.3 ± 1.2
WGDN _N	80.1 ± 1.2	67.4 ± 1.0	79.1 ± 2.5	81.9 ± 1.6	88.9 ± 0.9	90.4 ± 0.6	92.1 ± 0.9
WGDN _H	81.1 ± 1.3	69.9 ± 1.2	79.7 ± 2.2	82.6 ± 1.7	90.2 ± 1.2	90.9 ± 0.7	93.1 ± 0.8
WGDN _P	81.7 ± 0.9	69.7 ± 1.2	79.3 ± 2.0	<u>82.3 ± 1.6</u>	90.3 ± 0.9	<u>90.5 ± 0.6</u>	93.3 ± 0.6
GCN	79.3 ± 1.5	63.6 ± 1.8	76.1 ± 1.9	82.2 ± 1.4	89.6 ± 0.8	90.2 ± 0.5	93.5 ± 0.4
GAT	78.2 ± 1.6	65.6 ± 1.5	75.7 ± 2.0	80.6 ± 1.8	88.8 ± 1.3	82.5 ± 1.3	91.4 ± 1.4

Baselines We compare WGDN against representative models from five different categories: (1) traditional models including Node2Vec [7], Graph2Vec [22], DeepWalk [26], (2) graph kernel models including Weisfeiler-Lehman sub-tree kernel (WL) [30], deep graph kernel (DGK) [45], (3) predictive SSL models including GAE [13], GCN_{AE} [50], GALA [24], GDN [17], (4) contrastive SSL models including DGI [36], MVGRL [8], GRACE [51], GMI [25], GCA [52], InfoGraph [33], GraphCL [48], JOAO [47], InfoGCL [43], and (5) semi-supervised models including GCN [14], GAT [35] and GIN [44].

Evaluation protocol We closely follow the evaluation protocol in recent SSL researches. For node classification, the node embedding is fed into a logistics regression classifier [36]. We run 50 trials with different seeds and report the mean classification accuracy with standard deviation. For graph classification, we feed the graph representation into a linear SVM, and report the mean 10-fold cross validation accuracy with standard deviation after 5 runs [43]. Please refer to Appendix E.2 for further details.

Experiment settings We use the official implementations for all baselines in node classification and follow the suggested hyperparameter settings, whereas graph classification results are obtained from original papers if available. We develop three variants of our proposed methods as WGDN_N with GCN kernel $g_c(\lambda_i) = 1 - \lambda_i$, WGDN_H with heat diffusion kernel $g_c(\lambda_i) = e^{-t\lambda_i}$ and WGDN_P with personalized pagerank kernel $g_c(\lambda_i) = \frac{\alpha}{1 - (1 - \alpha)(1 - \lambda_i)}$. We use diffusion time $t = 1$ and teleport probability $\alpha = 0.2$. For wiener kernel approximation, the polynomial order K of WGDN_N is 9 while others are 2. All models are initialized using Glorot initialization [6] and optimized by Adam optimizer [12]. For node classification, early stopping is also employed with a patience of 20. Further details of model configurations can be found in Appendix E.3.

5.2 Performance comparison (Q1)

The node classification performance are reported in Table 1. We find that all variants of WGDN outperform the predictive SSL methods by a large margin over all datasets. The significant improvement verifies the effectiveness of our training scheme when applied to predictive SSL models. In addition, WGDN performs competitively with contrastive SSL methods, achieving state-of-the-art performances in 5 out of 7 datasets. For instance, our model WGDN is able to improve by a margin up to 4.7% on accuracy over the most outstanding contrastive method GRACE on Computers. Moreover, when compared to semi-supervised models, WGDN outperforms GCN in almost all datasets except Physics.

Table 2: Graph classification accuracy of all compared methods. The compared results are from the previous papers, and * indicates result is not reported.

Model	IMDB-B	IMDB-M	PROTEINS	COLLAB	MUTAG	DD	NCI1
WL	72.30 ± 3.44	46.95 ± 0.46	72.92 ± 0.56	*	80.72 ± 3.00	*	80.01 ± 0.50
DGK	66.96 ± 0.56	44.55 ± 0.52	73.30 ± 0.82	*	87.44 ± 2.72	*	80.31 ± 0.46
Graph2Vec	71.10 ± 0.54	50.44 ± 0.87	73.30 ± 2.05	*	83.15 ± 9.25	*	73.22 ± 1.81
MVGRL	74.20 ± 0.70	51.20 ± 0.50	*	*	89.70 ± 1.10	*	*
InfoGraph	73.03 ± 0.87	49.69 ± 0.53	74.44 ± 0.31	70.65 ± 1.13	89.01 ± 1.13	72.85 ± 1.78	76.20 ± 1.06
GraphCL	71.14 ± 0.44	48.58 ± 0.67	74.39 ± 0.45	71.36 ± 1.15	86.80 ± 1.34	78.62 ± 0.40	77.87 ± 0.41
JOAO	70.21 ± 3.08	49.20 ± 0.77	74.55 ± 0.41	69.50 ± 0.36	87.35 ± 1.02	77.32 ± 0.54	78.07 ± 0.47
InfoGCL	75.10 ± 0.90	51.40 ± 0.80	*	80.00 ± 1.30	91.20 ± 1.30	*	80.20 ± 0.60
WGDN _N	75.56 ± 0.32	51.57 ± 0.37	75.32 ± 0.26	80.96 ± 0.32	88.30 ± 1.33	79.46 ± 0.41	79.18 ± 0.32
WGDN _H	76.08 ± 0.50	51.80 ± 0.39	76.03 ± 0.40	81.26 ± 0.23	88.72 ± 1.02	79.46 ± 0.11	79.72 ± 0.39
WGDN _P	75.72 ± 0.20	51.80 ± 0.55	75.94 ± 0.66	81.50 ± 0.21	89.04 ± 0.21	79.00 ± 0.31	80.31 ± 0.25
GCN	74.0 ± 3.4	51.9 ± 3.8	*	79.0 ± 1.8	85.6 ± 5.8	*	80.2 ± 2.0
GIN	75.1 ± 5.1	52.3 ± 2.8	76.2 ± 2.8	80.2 ± 1.9	89.4 ± 5.6	*	82.7 ± 1.7

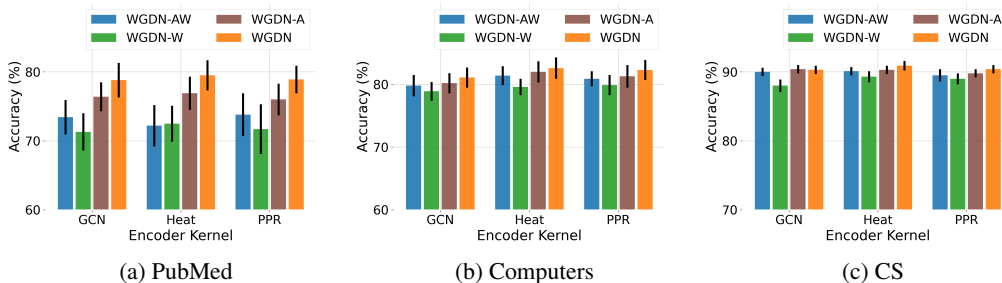


Figure 3: Node classification accuracy of models with and without key components (wiener decoder/latent augmentation). Complete training scheme consistently boosts model performance across different encoder types and datasets.

Table 2 lists the graph classification performance across various methods. We observe that our approach outperforms all SSL baselines in 6 out of 7 datasets. In the meantime, WGDN achieves greater results over the best kernel methods. Even when compared to semi-supervised models, our model achieves the best results in 2 out of 7 datasets and the gaps for the rest are minor.

In summary, regardless of the encoder types, our model consistently achieves comparable performance with the cutting-edge SSL and semi-supervised methods across node-level and graph-level tasks, which demonstrates the effectiveness and flexibility of WGDN under SSL framework.

5.3 Effectiveness of key components (Q2)

To validate the benefit of introducing latent augmentation and graph wiener decoder, we conduct ablation studies on three datasets in node classification that exhibit distinct characteristics (e.g., citation, co-purchase and co-author). For clarity, WGDN-A and WGDN-W are denoted as the models removing augmentation or substituting wiener decoder with inverse decoder. WGDN-AW is the plain model without both components. Considering the trivial inverse of GCN is intractable, we use GALA [24] instead.

From Figure 3, we make several observations. **(1)** WGDN-W consistently underperform WGDN-AW. This observation validates that deterministic inverse decoder fails to retrieve useful information from augmented low-dimensional embedding, which is consistent with our theoretical analysis in Section 4.1. **(2)** Compared with WGDN-AW, WGDN-A improves model performance across various encoder types and datasets, which suggests that graph wiener decoder may provide more insights in representation learning. **(3)** The performance of WGDN is significantly higher than other counterparts. For instance, WGDN has a relative improvement up to 6% over WGDN-AW on PubMed regardless of the encoder types. It can be concluded that the combination of augmentation and wiener decoder allows the model to generate more semantic embedding from the augmented latent space.

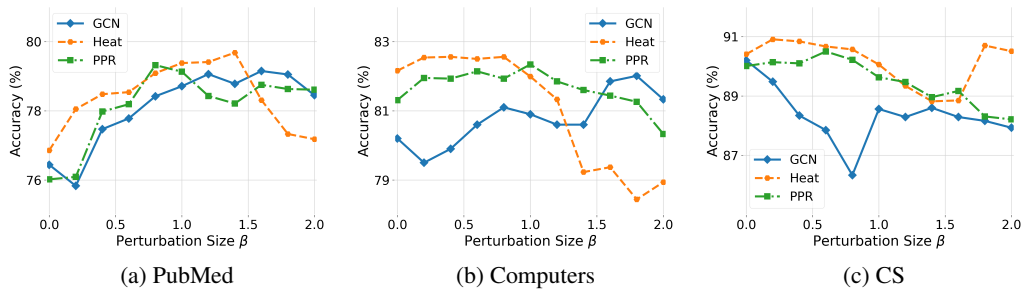


Figure 4: Node classification accuracy with varied augmentation size β .

5.4 Scalability analysis (Q3)

Note that scalability is a big concern in most contrastive SSL methods. The complex data augmentation schemes tend to cause scaling-up issues, while WGDN can be efficiently implemented as discussed in Section 4.2. We empirically evaluate the computational cost in GPU over four large datasets. To have fair comparisons, the embedding size of all models is set to 512. It is evident from Table 3 that the memory requirement of WGDN is significantly reduced

up to 8x without sacrificing model performance. In particular, the scalability of WGDN is more prominent on large-scale dataset such as Physics. Considering that memory is usually the bottleneck in graph-based applications, WGDN demonstrates a practical advantage over prior methods when limited resources are available.

Table 3: Computational requirements on benchmark datasets. * denotes Out-of-Memory on a Tesla V100 32G GPU.

Model	PubMed	Computers	CS	Physics
GRACE	12.57 GB	8.35 GB	12.92 GB	31.04 GB
GMI	22.81 GB	15.42 GB	23.61 GB	*
WGDN	2.72 GB	4.52 GB	6.84 GB	12.37 GB

5.5 Hyperparameter analysis (Q4)

Augmentation size β It is expected that introducing adequate augmentation enriches the diversity of samples in the latent space, which contributes to learning more expressive representations. To validate this, we conduct experiments varying β from 0 to 2. Figure 4 shows that the classification accuracy generally reaches the peak and drops gradually when the augmentation size β increases, which aligns with our intuition. However, it is worth noting that augmenting latent space may lead to performance degradation for certain circumstances such as GCN encoder on CS. Overall, the trend verifies the effectiveness of introducing latent augmentation in representation learning.

Convolution filter g_c Table 1 and 2 shows the influence of different convolution filters. It is observed that diffusion based WGDN outperforms its trivial version with GCN filter across node and graph applications. In addition, we also find that training loss of diffusion models is significantly smaller. Both phenomena verify that graph diffusion can provide both meaningful aggregation and powerful reconstruction to improve representation learning.

6 Conclusion and future work

In this paper, we propose Wiener Graph Deconvolutional Network (WGDN), a predictive self-supervised learning framework for graph-structured data. By introducing simple latent augmentations, our model can efficiently learn semantic representations from the augmented latent space along with graph wiener decoder. We provide a theoretical analysis for the superiority of reconstruction ability and efficacy of graph wiener filter. Extensive experimental results on various datasets demonstrate that our proposed WGDN achieves competitive performance over unsupervised counterparts, and even outperforms several semi-supervised architectures. Our work shows the great potentials of latent data augmentations and predictive SSL in representation learning, and more in-depth explorations will be conducted in future work.

References

- [1] Richard L Burden, J Douglas Faires, and Annette M Burden. *Numerical analysis*. Cengage learning, 2015.
- [2] Tsz-Him Cheung and Dit-Yan Yeung. MODALS: Modality-agnostic automated data augmentation in the latent space. In *ICLR*, 2021.
- [3] Terrance DeVries and Graham W Taylor. Dataset augmentation in feature space. *arXiv preprint arXiv:1702.05538*, 2017.
- [4] Jiangxin Dong, Stefan Roth, and Bernt Schiele. Deep wiener deconvolution: Wiener meets deep learning for image deblurring. In *NeurIPS*, 2020.
- [5] Johannes Gasteiger, Aleksandar Bojchevski, and Stephan Günnemann. Combining neural networks with personalized pagerank for classification on graphs. In *ICLR*, 2019.
- [6] Xavier Glorot and Yoshua Bengio. Understanding the difficulty of training deep feedforward neural networks. In *AISTATS*, 2010.
- [7] Aditya Grover and Jure Leskovec. node2vec: Scalable feature learning for networks. In *KDD*, 2016.
- [8] Kaveh Hassani and Amir Hosein Khasahmadi. Contrastive multi-view representation learning on graphs. In *ICML*, 2020.
- [9] Weihua Hu, Bowen Liu, Joseph Gomes, Marinka Zitnik, Percy Liang, Vijay Pande, and Jure Leskovec. Strategies for pre-training graph neural networks. In *ICLR*, 2020.
- [10] Sergey Ioffe and Christian Szegedy. Batch normalization: Accelerating deep network training by reducing internal covariate shift. In *ICML*, 2015.
- [11] Hongwei Jin and Xinhua Zhang. Latent adversarial training of graph convolutional networks. In *ICML workshop on Learning and Reasoning with Graph-Structured Representations*, 2019.
- [12] Diederik P Kingma and Jimmy Ba. Adam: A method for stochastic optimization. In *ICLR*, 2015.
- [13] Thomas N Kipf and Max Welling. Variational graph auto-encoders. In *NeurIPS Workshop on Bayesian Deep Learning*, 2016.
- [14] Thomas N. Kipf and Max Welling. Semi-supervised classification with graph convolutional networks. In *ICLR*, 2017.
- [15] Johannes Klicpera, Stefan Weissenberger, and Stephan Günnemann. Diffusion improves graph learning. In *NeurIPS*, 2019.
- [16] Varun Kumar, Hadrien Glaude, Cyprien de Lichy, and William Campbell. A closer look at feature space data augmentation for few-shot intent classification. In *EMNLP Workshop on Deep Learning Approaches for Low-Resource NLP*, 2019.
- [17] Jia Li, Jiajin Li, Yang Liu, Jianwei Yu, Yueting Li, and Hong Cheng. Deconvolutional networks on graph data. In *NeurIPS*, 2021.
- [18] Yuening Li, Xiao Huang, Jundong Li, Mengnan Du, and Na Zou. Specac: Spectral autoencoder for anomaly detection in attributed networks. In *CIKM*, 2019.
- [19] Xiaofeng Liu, Yang Zou, Lingsheng Kong, Zhihui Diao, Junliang Yan, Jun Wang, Site Li, Ping Jia, and Jane You. Data augmentation via latent space interpolation for image classification. In *ICPR*, 2018.
- [20] Yixin Liu, Shirui Pan, Ming Jin, Chuan Zhou, Feng Xia, and Philip S Yu. Graph self-supervised learning: A survey. *IEEE Transactions on Knowledge and Data Engineering*, 2022.
- [21] Christopher Morris, Nils M. Kriege, Franka Bause, Kristian Kersting, Petra Mutzel, and Marion Neumann. Tudataset: A collection of benchmark datasets for learning with graphs. In *ICML Workshop on Graph Representation Learning and Beyond*, 2020.
- [22] Annamalai Narayanan, Mahinthan Chandramohan, Rajasekar Venkatesan, Lihui Chen, Yang Liu, and Shantanu Jaiswal. graph2vec: Learning distributed representations of graphs. *arXiv preprint arXiv:1707.05005*, 2017.
- [23] Ricardo Pachon and Lloyd Trefethen. Barycentric-remez algorithms for best polynomial approximation in the chebfun system. *BIT*, 2009.

- [24] Jiwoong Park, Minsik Lee, Hyung Jin Chang, Kyuewang Lee, and Jin Young Choi. Symmetric graph convolutional autoencoder for unsupervised graph representation learning. In *ICCV*, 2019.
- [25] Zhen Peng, Wenbing Huang, Minnan Luo, Qinghua Zheng, Yu Rong, Tingyang Xu, and Junzhou Huang. Graph Representation Learning via Graphical Mutual Information Maximization. In *WWW*, 2020.
- [26] Bryan Perozzi, Rami Al-Rfou, and Steven Skiena. Deepwalk: Online learning of social representations. In *KDD*, 2014.
- [27] Nathanaël Perraudin and Pierre Vandergheynst. Stationary signal processing on graphs. *IEEE Transactions on Signal Processing*, 2017.
- [28] Prithviraj Sen, Galileo Namata, Mustafa Bilgic, Lise Getoor, Brian Galligher, and Tina Eliassi-Rad. Collective classification in network data. *AI magazine*, 2008.
- [29] Oleksandr Shchur, Maximilian Mumme, Aleksandar Bojchevski, and Stephan Günnemann. Pitfalls of graph neural network evaluation. In *NeurIPS Workshop on Relational Representation Learning*, 2018.
- [30] Nino Shervashidze, Pascal Schweitzer, Erik Jan Van Leeuwen, Kurt Mehlhorn, and Karsten M Borgwardt. Weisfeiler-lehman graph kernels. *JMLR*, 2011.
- [31] Hyeonseok Son and Seungyong Lee. Fast non-blind deconvolution via regularized residual networks with long/short skip-connections. In *ICCP*, 2017.
- [32] David Stutz, Matthias Hein, and Bernt Schiele. Disentangling adversarial robustness and generalization. In *CVPR*, 2019.
- [33] Fan-Yun Sun, Jordan Hoffman, Vikas Verma, and Jian Tang. Infograph: Unsupervised and semi-supervised graph-level representation learning via mutual information maximization. In *ICLR*, 2019.
- [34] Paul Upchurch, Jacob Gardner, Geoff Pleiss, Robert Pless, Noah Snavely, Kavita Bala, and Kilian Weinberger. Deep feature interpolation for image content changes. In *CVPR*, 2017.
- [35] Petar Veličković, Guillem Cucurull, Arantxa Casanova, Adriana Romero, Pietro Liò, and Yoshua Bengio. Graph Attention Networks. In *ICLR*, 2018.
- [36] Petar Veličković, William Fedus, William L Hamilton, Pietro Liò, Yoshua Bengio, and R Devon Hjelm. Deep graph infomax. In *ICLR*, 2019.
- [37] Vikas Verma, Alex Lamb, Christopher Beckham, Amir Najafi, Ioannis Mitliagkas, David Lopez-Paz, and Yoshua Bengio. Manifold mixup: Better representations by interpolating hidden states. In *ICML*, 2019.
- [38] Chun Wang, Shirui Pan, Guodong Long, Xingquan Zhu, and Jing Jiang. Mgae: Marginalized graph autoencoder for graph clustering. In *CIKM*, 2017.
- [39] Haonan Wang, Jieyu Zhang, Qi Zhu, and Wei Huang. Augmentation-free graph contrastive learning. *arXiv preprint arXiv:2204.04874*, 2022.
- [40] Norbert Wiener. *Extrapolation, Interpolation, and Smoothing of Stationary Time Series*. The MIT Press, 1964.
- [41] Felix Wu, Amauri Souza, Tianyi Zhang, Christopher Fifty, Tao Yu, and Kilian Weinberger. Simplifying graph convolutional networks. In *ICML*, 2019.
- [42] Yaochen Xie, Zhao Xu, Jingtun Zhang, Zhengyang Wang, and Shuiwang Ji. Self-supervised learning of graph neural networks: A unified review. *IEEE Transactions on Pattern Analysis and Machine Intelligence*, 2022.
- [43] Dongkuan Xu, Wei Cheng, Dongsheng Luo, Haifeng Chen, and Xiang Zhang. Infogcl: Information-aware graph contrastive learning. In *NeurIPS*, 2021.
- [44] Keyulu Xu, Weihua Hu, Jure Leskovec, and Stefanie Jegelka. How powerful are graph neural networks? In *ICLR*, 2019.
- [45] Pinar Yanardag and SVN Vishwanathan. Deep graph kernels. In *KDD*, 2015.
- [46] Jingkan Yang and Santiago Segarra. Enhancing geometric deep learning via graph filter deconvolution. In *GlobalSIP*, 2018.

- [47] Yuning You, Tianlong Chen, Yang Shen, and Zhangyang Wang. Graph contrastive learning automated. In *ICML*, 2021.
- [48] Yuning You, Tianlong Chen, Yongduo Sui, Ting Chen, Zhangyang Wang, and Yang Shen. Graph contrastive learning with augmentations. In *NeurIPS*, 2020.
- [49] Yuning You, Tianlong Chen, Zhangyang Wang, and Yang Shen. When does self-supervision help graph convolutional networks? In *ICML*, 2020.
- [50] Chun-Yang Zhang, Junfeng Hu, Lin Yang, CL Philip Chen, and Zhiliang Yao. Graph deconvolutional networks. *Information Sciences*, 2020.
- [51] Yanqiao Zhu, Yichen Xu, Feng Yu, Qiang Liu, Shu Wu, and Liang Wang. Deep Graph Contrastive Representation Learning. In *ICML Workshop on Graph Representation Learning and Beyond*, 2020.
- [52] Yanqiao Zhu, Yichen Xu, Feng Yu, Qiang Liu, Shu Wu, and Liang Wang. Graph contrastive learning with adaptive augmentation. In *WWW*, 2021.

A Proof of Proposition 4.1

Proof. By substitution, $\hat{\mathbf{x}}_{inv} = \mathbf{x} + \mathbf{U}g_d(\mathbf{\Lambda})\mathbf{U}^T\epsilon$. Note that MSE is reduced to

$$\mathbb{E}\|\mathbf{x} - \hat{\mathbf{x}}_{inv}\|_2^2 = \mathbb{E}\|\mathbf{U}g_d(\mathbf{\Lambda})\mathbf{U}^T\epsilon\|_2^2 = \sum_{i=1}^N \frac{\sigma^2}{g_c^2(\lambda_i)}. \quad (16)$$

Regarding the condition $g_c : [0, 2] \mapsto [-1, 1]$, we take GCN where $g_c(\lambda_i) = 1 - \lambda_i$ as a representative example. By substitution, we have

$$\mathbb{E}\|\mathbf{x} - \hat{\mathbf{x}}_{inv}\|_2^2 = \sum_{i=1}^N \frac{\sigma^2}{(1 - \lambda_i)^2}, \quad (17)$$

and $\frac{1}{(1-\lambda_i)^2} \rightarrow \infty$ when $\lambda_i \rightarrow 1$. □

B Proof of Proposition 4.2

Proof. By the definition of $g_w(\lambda_i)$

$$\begin{aligned} \mathbb{E}\|\mathbf{x} - \hat{\mathbf{x}}_w\|_2^2 &= \sum_{i=1}^N \frac{\sigma^2(g_c^2(\lambda_i) + \sigma^2/\mathbb{E}[x_i^{*2}])}{(g_c^2(\lambda_i) + \sigma^2/\mathbb{E}[x_i^{*2}])^2} \\ &= \sum_{i=1}^N \frac{\sigma^2}{g_c^2(\lambda_i) + \sigma^2/\mathbb{E}[x_i^{*2}]} \\ &\leq \sum_{i=1}^N \frac{\sigma^2}{g_c^2(\lambda_i)}. \end{aligned} \quad (18)$$

Plugging in the inverse filter, we can obtain

$$\begin{aligned} \sum_{i=1}^N \text{VAR}[\hat{\mathbf{x}}_{inv,i}] &= \text{Tr}(\text{COV}[\hat{\mathbf{x}}_{inv}]) \\ &= \text{Tr}(\text{COV}[\mathbf{U}\mathbf{x}^*] + \text{COV}[\mathbf{U}g_d(\mathbf{\Lambda})\epsilon^*]) \\ &= \sum_{i=1}^N (\text{VAR}[\mathbf{x}_i^*] + \frac{\sigma^2}{g_c^2(\lambda_i)}), \end{aligned} \quad (19)$$

where Tr represents the matrix trace. Similarly, variance of $\hat{\mathbf{x}}_w$ is convoluted by $g_w(\lambda_i)$

$$\begin{aligned} \sum_{i=1}^N \text{VAR}[\hat{\mathbf{x}}_{w,i}] &= \text{Tr}(\text{COV}[\hat{\mathbf{x}}_w]) \\ &= \sum_{i=1}^N \left[\frac{g_c^2(\lambda_i)}{g_c^2(\lambda_i) + \sigma^2/\mathbb{E}[x_i^{*2}]} \right]^2 (\text{VAR}[\mathbf{x}_i^*] + \frac{\sigma^2}{g_c^2(\lambda_i)}) \\ &\leq \sum_{i=1}^N (\text{VAR}[\mathbf{x}_i^*] + \frac{\sigma^2}{g_c^2(\lambda_i)}). \end{aligned} \quad (20)$$

□

C Proof of Proposition 4.3

Proof. Similar to Appendix B, variance of $\hat{\mathbf{x}}_{w,\gamma}$ is reduced to

$$\begin{aligned} \sum_{i=1}^N \text{VAR}(\hat{\mathbf{x}}_{w,\gamma,i}) &= \text{Tr}(\text{COV}(\hat{\mathbf{x}}_{w,\gamma})) \\ &= \sum_{i=1}^N \left[\frac{g_c^2(\lambda_i)}{g_c^2(\lambda_i) + \sigma^2/x_\gamma^{*2}} \right]^2 (\text{VAR}[\mathbf{x}_i^*] + \frac{\sigma^2}{g_c^2(\lambda_i)}) \\ &\leq \sum_{i=1}^N (\text{VAR}[\mathbf{x}_i^*] + \frac{\sigma^2}{g_c^2(\lambda_i)}). \end{aligned} \quad (21)$$

For the specific spectrum λ_i where $\mathbb{E}[x_i^{*2}] \leq \bar{x}_\gamma^{*2}$ holds, the spectral reconstruction error satisfies

$$\begin{aligned} S(\lambda_i, x_i^*, \sigma, g_c, \bar{g}_{w,\gamma}) &= \frac{1}{(g_c^2(\lambda_i) + \sigma^2/\bar{x}_\gamma^{*2})^2} \left[\sigma^2 (g_c^2(\lambda_i) + \frac{\sigma^2}{\bar{x}_\gamma^{*2}} \times \frac{\mathbb{E}[x_i^{*2}]}{\bar{x}_\gamma^{*2}}) \right] \\ &\leq \frac{1}{(g_c^2(\lambda_i) + \sigma^2/\bar{x}_\gamma^{*2})^2} \left[\sigma^2 (g_c^2(\lambda_i) + \frac{\sigma^2}{\bar{x}_\gamma^{*2}}) \right] \\ &= \frac{\sigma^2}{g_c^2(\lambda_i) + \sigma^2/\bar{x}_\gamma^{*2}} \\ &\leq \frac{\sigma^2}{g_c^2(\lambda_i)} = S(\lambda_i, x_i^*, \sigma, g_c, g_c^{-1}). \end{aligned} \quad (22)$$

Note that the second derivative of spectral reconstruction error $S(\lambda_i, x_i^*, \sigma, g_c, g_d)$ with respect to $g_d(\lambda_i)$ is

$$\frac{\partial^2}{\partial g_d^2(\lambda_i)} S(\lambda_i, x_i^*, \sigma, g_c, g_d) = 2(g_c^2(\lambda_i) \mathbb{E}[x_i^{*2}] + \sigma^2) \geq 0, \quad (23)$$

thus, $S(\lambda_i, x_i^*, \sigma, g_c, g_d)$ is a convex function. By Eq. 6, $g_w(\lambda_i)$ is the solution for global minimum. By convexity, for any filter $g_d(\lambda_i)$, the value of $S(\lambda_i, x_i^*, \sigma, g_c, g_d)$ is greater when distance to global minimizer $|g_d(\lambda_i) - g_w(\lambda_i)|$ is larger. Considering $\bar{g}_{w,\gamma}(\lambda_i)$, it can be reduced to

$$|\bar{g}_{w,\gamma}(\lambda_i) - g_w(\lambda_i)| = |g_c(\lambda_i)| \times \left| \frac{1}{g_c^2(\lambda_i) + \sigma^2/\bar{x}_\gamma^{*2}} - \frac{1}{g_c^2(\lambda_i) + \sigma^2/\mathbb{E}[x_i^{*2}]} \right|. \quad (24)$$

Given the condition that $x_i^{*2} \leq \bar{x}_{\gamma_1}^{*2} \leq \bar{x}_{\gamma_2}^{*2}$, we can conclude that

$$|\bar{g}_{w,\gamma_1}(\lambda_i) - g_w(\lambda_i)| \leq |\bar{g}_{w,\gamma_2}(\lambda_i) - g_w(\lambda_i)|. \quad (25)$$

Therefore, $S(\lambda_i, x_i^*, \sigma, g_c, \bar{g}_{w,\gamma_1}) \leq S(\lambda_i, x_i^*, \sigma, g_c, \bar{g}_{w,\gamma_2}) \leq S(\lambda_i, x_i^*, \sigma, g_c, g_c^{-1})$ holds. \square

D Details of Model Architecture

RSNR estimation Let $\hat{\mathbf{H}}^{(m)}$ denotes the input of m -th layer decoder, the average spectral power $\bar{x}_{\gamma_i}^{*2}$ in $\mathbf{D}_{\gamma_i}^{(m)}$ is estimated by

$$\bar{x}_{\gamma_i}^{*2} = \frac{\gamma_i}{ND'} \left(\left\| \hat{\mathbf{H}}^{(m)} \right\|_F^2 + \left\| \hat{\mathbf{H}}^{(m)} - \frac{1}{N} \mathbb{1} \hat{\mathbf{H}}^{(m)} \right\|_F^2 \right), \quad (26)$$

where $\mathbb{1} \in \mathbb{R}^{N \times D'}$ is the all ones matrix and D' is the size of hidden space. The augmentation variance σ^2 is estimated by considering its neighborhood as

$$\sigma^2 = \frac{1}{ND'} \left\| \hat{\mathbf{H}}^{(m)} - \mathbf{A} \hat{\mathbf{H}}^{(m)} \right\|_F^2 \quad (27)$$

Skip connection To learn more expressive representations, skip connection is considered as it transmits aggregated information to decoder for better reconstruction. If skip connection is implemented, we let $\hat{\mathbf{H}}_d^{(m)} = \hat{\mathbf{H}}^{(m)}$ for clarity. For $m = 1, \dots, M - 1$, we augment the output of the m -layer encoder, denoted as $\hat{\mathbf{H}}_e^{(m)}$, by

$$\hat{\mathbf{H}}_e^{(m)} = \mathbf{H}^{(m)} + \beta \mathbf{E}^{(m)}, \quad (28)$$

where $\mathbf{E}^{(m)} = \{\epsilon_1^{(m)}, \dots, \epsilon_N^{(m)}\}$, $\epsilon_i^{(m)} \sim N(\mathbf{0}, \sigma_P^2(m) \mathbf{I})$, $\sigma_P^2(m) = \text{VAR}[\mathbf{H}^{(m)}]$ and β is same hyperparameter in Eq. 13. Both augmented representations are fed into the decoder as

$$\begin{aligned} \mathbf{Z}_{i,s}^{(m-1)} &= \phi(\mathbf{D}_{\gamma_i,s}^{(m)} \hat{\mathbf{H}}_s^{(m)} \mathbf{W}_i^{(m)}), \\ \hat{\mathbf{H}}_s^{(m-1)} &= \text{AGG}([\mathbf{Z}_{1,s}^{(m-1)}, \dots, \mathbf{Z}_{q,s}^{(m-1)}]), \end{aligned} \quad (29)$$

where $s = \{e, d\}$ represents the source. The final representation of m -layer decoder is obtained by averaging the intermediate embeddings,

$$\hat{\mathbf{H}}^{(m-1)} = \text{AVG}(\hat{\mathbf{H}}_e^{(m-1)}, \hat{\mathbf{H}}_d^{(m-1)}). \quad (30)$$

For graph classification, we apply batch normalization [10] right before activation function for all layers except the final prediction layer.

E Detailed Experimental Setup

E.1 Datasets Splitting

We closely follow the random split mechanism suggested in [5]. To conduct comprehensive evaluation on node classification, each dataset is divided into a development set and a test set with fixed seed. Specifically, 1500 nodes are randomly sampled as development set for all dataset except Coauthor Physics, in which 5000 nodes are sampled. For each run, the development set is randomly split into a training set which includes 20 nodes per class and a validation set with the remaining nodes. To ensure model reproducibility, random seeds are drawn once in advance and fixed across runs to facilitate comparisons.

E.2 Evaluation Protocol

For unsupervised methods, all the resulted embedding from well-trained models are frozen. For node classification tasks, we use Glorot initialization [6] to initialize model parameters and all downstream models are trained for 300 epochs by Adam optimizer [12] with a learning rate 0.01. For semi-supervised methods, to conduct fair comparisons, we follow the same settings as unsupervised methods and employ 2-layer encoders with embedding size 512 for both GCN [14] and GAT [35]. Specifically, the first layer of GAT consists of 2 heads and the second layer has 1 output head. We run 50 trials and keep the model with the highest performance in validation set as final. For graph classification tasks, linear SVM is fine-tuned with grid search on C parameter from $\{10^{-3}, 10^{-2}, \dots, 1, 10\}$.

E.3 Hyperparameter Specifications

By default, wiener graph decoder is implemented with multiple channels with $q = 3$ and $\gamma = [0.1, 1, 10]$. Otherwise, single channel is used with $\gamma = 1$. The specific hyperparameter configurations are illustrated in Table 5 and 6.

E.4 Computational Hardware

We use the machine with the following configurations for all model training and evaluation.

- OS: Ubuntu 20.04.1 LTS
- CPU: Intel(R) Xeon(R) Silver 4114 CPU @ 2.20GHz
- GPU: NVIDIA Tesla V100, 32GB

Table 4: Summary of datasets for graph representation learning

	Cora	CiteSeer	PubMed	Computers	Photo	CS	Physics
Nodes	2,708	3,327	19,717	13,752	7,650	18,333	34,493
Edges	10,556	9,104	88,648	491,722	238,162	163,788	495,924
Classes	7	6	3	10	8	15	5
Features	1,433	3,703	500	767	745	8,415	8,415

	IMDB-B	IMDB-M	PROTEINS	COLLAB	MUTAG	DD	NCII
Graphs	1,000	1,500	1,113	5,000	188	1,178	4,110
Avg. Nodes	19.77	13.00	39.06	74.49	17.93	284.32	29.87
Avg. Edges	193.06	65.94	72.82	2457.78	19.79	715.66	32.30
Classes	2	3	2	3	2	2	2
Node Labels	-	-	✓	-	✓	✓	✓

Table 5: Detailed hyperparameter configurations for node classification

Kernel	Dataset	β	Aggregation	Learning rate	Hidden dimension	Layer	Single channel	Skip connection
GCN	Cora	1.5	Sum	0.01	512	2	-	-
	CiteSeer	2.0	Sum				-	✓
	PubMed	1.6	Avg				-	✓
	Computers	1.8	Sum				-	-
	Photo	0.1	-				✓	✓
	CS	0.1	Sum				-	✓
	Physics	1.0	Sum				-	✓
Heat	Cora	1.4	Max	0.01	512	2	-	-
	CiteSeer	2.2	Avg				-	✓
	PubMed	1.4	Avg				-	✓
	Computers	0.2	-				✓	✓
	Photo	0.1	-				✓	✓
	CS	0.2	-				✓	✓
	Physics	1.0	Sum				-	✓
PPR	Cora	1.0	Max	0.01	512	2	-	-
	CiteSeer	1.3	Sum				-	✓
	PubMed	0.8	Avg				-	✓
	Computers	1.0	-				✓	✓
	Photo	0.2	-				✓	✓
	CS	0.6	-				✓	✓
	Physics	1.0	Sum				-	✓

Table 6: Detailed hyperparameter configurations for graph classification

Kernel	Dataset	β	Aggregation	Pooling	Learning rate	Hidden dimension	Batch size	Epoch	Layer	Single channel	Skip connection
GCN	IMDB-B	1.5	Max	Avg	0.0001	512	32	60	2	-	✓
	IMDB-M	1.0	-	Avg				50	2	✓	✓
	PROTEINS	1.0	Sum	Max				100	3	-	-
	COLLAB	1.0	-	Max	0.0005	32	64	20	2	✓	✓
	MUTAG	1.0	Sum	Sum				20	3	-	✓
	DD	1.0	Max	Sum				0.0001	512	32	100
	NCI1	1.0	-	Max	0.0005	512	16	300	2	✓	-
Heat	IMDB-B	1.5	Max	Avg	0.0001	512	32	30	2	-	✓
	IMDB-M	1.0	-	Avg				50	2	✓	✓
	PROTEINS	1.0	-	Max				90	3	✓	✓
	COLLAB	1.0	-	Max	0.0005	32	64	20	2	✓	✓
	MUTAG	1.6	Avg	Sum				20	2	-	✓
	DD	1.0	Avg	Sum				0.0001	512	32	100
	NCI1	0.5	-	Max	0.0005	512	16	150	2	✓	-
PPR	IMDB-B	1.5	Max	Avg	0.0001	512	32	30	2	-	✓
	IMDB-M	1.0	Sum	Avg				50	3	✓	-
	PROTEINS	1.0	Avg	Max				100	3	-	✓
	COLLAB	1.0	-	Max	0.0005	32	64	20	2	✓	✓
	MUTAG	1.2	Sum	Sum				20	2	-	-
	DD	1.0	Avg	Sum				0.0001	512	32	100
	NCI1	1.0	-	Max	0.0005	512	16	100	2	✓	✓